Front. Environ. Sci. Eng. 2015, 9(5): 770–783
DOI 10.1007/s11783-015-0811-0

REVIEW ARTICLE

Applications of hollow nanomaterials in environmental remediation and monitoring: A review

Yuankai ZHANG, Zhijiang HE, Hongchen WANG (✉), Lu QI, Guohua LIU, Xiaojun ZHANG

School of Environment & Natural Resource, Renmin University of China, Beijing 100872, China

Abstract Hollow nanomaterials have attracted significant attention because of their high chemical and thermal stability, high specific surface area, high porosity, low density, and good biocompatibility. These state-of-the-art nanomaterials have been shown to efficiently adsorb heavy metals, and volatile hazardous substances, photodegrade persistent organic pollutants, and other compounds, and inactivate bacteria. Such properties have enabled the use of these materials for environmental remediation, such as in water/wastewater treatment, soil remediation, air purification, and substance monitoring, etc. Hollow nanomaterials showed higher photocatalytic activity than those without hollow structure owing to their high active surface area, reduced diffusion resistance, and improved accessibility. And, the Doping method could improve the photocatalytic performance of hollow nanomaterials further under visible light. Moreover, the synthetic mechanisms and methods of these materials are important because their size and morphology help to determine their precise properties. This article reviews the environmental applications and potential risks of these materials, in addition to their syntheses. Finally, an outlook into the development of these materials is provided.

Keywords hollow nanomaterials, environmental remediation, nanotechnology, nanostructures, morphology

1 Introduction

The growth of the world economy has been accompanied by significant environmental deterioration. For example, water, soil, and air have been severely polluted by toxic heavy metal ions (HMIs), dyes, persistent organic pollutants (POPs), and others. According to a World Bank investigation, between 8% and 12% of China's gross domestic product is consumed in resolving environmental damage every year [1]. Therefore, a low-cost, energy-saving, and environmentally friendly method for environmental remediation is urgently required in order to maintain rapid economic development without further damaging the environment, especially in developing countries. In recent years, nanoscience has provided new ways to revolutionize the world around us and nano-sized materials have contributed to solving various modern environmental issues [2]. For example, nano-sized materials can be used to effectively treat the contaminated soils, sediments, and solid wastes, and also contribute to the improved treatment of water, wastewater, or noxious gas when anchored onto a solid matrix such as activated carbon and/or zeolite [3]. These materials, and nanomaterials in general, derive their unique properties from their unusual size, as they are restricted to be smaller than 100 nm in at least one dimension and potentially as small as the atomic and molecular length scales (~0.2 nm) [4].

Heavy metals and organic contaminants threaten human health and living organisms as a result of environmental pollution. Hollow nanomaterials were first synthesized in 1974 by Aldinger [5]. Due to their excellent properties, high chemical and thermal stability, high specific surface area, high porosity, low density, and good biocompatibility [6], hollow nanomaterials show promise in environmental remediation applications. For example, hollow silicate nanostructures showed an excellent ability to remove Pb^{2+} from contaminated water owing to their large specific surface area and unique structure [7]. Meanwhile, Liu et al. [8] found that hollow CuO spheres showed excellent and rapid photocatalytic degradation of dyes, especially for methyl blue (MB). Furthermore, mesoporous TiO_2/SiO_2 composite nanofibers have been able to decompose methylene blue, active yellow, and disperse red selectively [9]. In addition, these materials are also very promising as sensors for detecting environmental toxins because of their high surface area and well-aligned nanoporous structures.

Received November 27, 2014; accepted July 28, 2015

E-mail: whc@ruc.edu.cn

Hollow nanomaterials mainly refer to nanotubes or nanoparticles with an internal cavity (or hollow spheres/non-spheres); they can take on different nanostructures as shown in Fig. 1(a). Complex hollow nanomaterials with unique multi-shelled structures and hierarchical architectures could be used to further improve their electrochemical performance and cycling stability. For example, Yu et al. [10] fabricated well-defined NiS nanoparticles with a box-in-box hollow structure that exhibited high specific capacitance, excellent rate capability and good cycling stability. A wide spectrum of organic or inorganic materials ranging from single elements (such as graphene [11]) to ternary compounds (such as YVO_4:Eu^{3+} [12]), and from metals (such as Pt [13]) to semiconductors (such as SiO_2 [14]) have been used to synthesize hollow nanomaterials. Furthermore, hollow nanomaterials can be classified as zero- (0D), one- (1D), two- (2D), or three-dimensional (3D) materials. Generally, 1D hollow nanostructures (such as nanowires and nanotubes) show superior stability owing to slight agglomeration, which allows for functionalization of their surfaces with target-specific receptor species [15]. 3D hollow nanostructures often have excellent physical properties, which impart them with superior electrocatalytic activity. Wang et al. [16] synthesized hierarchical hollow urchins of $NiCo_2O_4$ (HU-$NiCo_2O_4$) using sulfonated-polystyrene (sulfonated-PS) as a hard template followed by thermal decomposition. The synthesized HU-$NiCo_2O_4$ had three levels of hierarchy, namely, 0D nanoparticle, 1D chain and, 3D hollow urchin structure. The fabrication process of HU-$NiCo_2O_4$ is schematically shown in Fig. 1(b) [16]. The urchin-like P-HU-$NiCo_2O_4$ particles were produced by slow addition of Na_2CO_3 after the adsorption of Ni^{2+} and Co^{2+}, from a solution of Ni$(NO_3)_2$ and Co$(NO_3)_2$, respectively, on the surface of sulfonated-PS particles. The sulfonated-PS particles were removed by calcination in air at 400°C for 6 h (Eq. (1)). This afforded HU-$NiCo_2O_4$ particles with a hierarchical hollow urchin-like structure. Thus, owing to its abundant diffusion paths, the well-connected 3D structure displayed superior electrocatalytic activity toward oxygen evolution processes with lower overpotential, higher current density, and higher stability as compared to other structures.

$$Ni_2CO_3(OH)_2 + 4Co(CO_3)_{0.5}(OH) + O_2 \rightarrow 2NiCo_2O_4 + 3CO_2\uparrow + 3H_2O\uparrow \quad (1)$$

Additionally, the number of research articles on hollow nanotechnology over 1991–2013 increased sharply with the year (from 1 in 1991 to 2226 in 2013); the trend in annual increment between the years is similar (arrived at 325 in 2013) (Fig. 1(c)). The data are based on an online search of SCI Expanded, i.e., Thomson Reuters "Web of science" with the key word "hollow nano*." Moreover, based on the analysis of all the hollow nanotechnology research articles over the year 1991–2013, as shown in Fig. 1(d), China had the highest counts (6408, 50.4%), followed by the United States (1958, 15.4%) and Japan (998, 7.9%). Thus, it is evident that research on hollow nanomaterials and their promising environmental applications is of great importance in China.

This review article focuses on the definition of hollow nanomaterials, the mechanism of hollow nanostructure formation and the application of hollow nanomaterials as detectors for the removal of HMIs and organic pollutants. In addition, the potential risks associated with these materials are discussed.

2 Applications in HMI removal

HMIs, such as Hg, Cu, Ni, and Cr are generally toxic and environmentally destructive even at very low concentrations, and are found as pollutants in groundwater, wastewater, soil, and even the air. The unique features of hollow nanomaterials have given them the ability to effectively adsorb or photodegrade large quantities of these pollutants.

2.1 HMIs removal by adsorption

Nanomaterials with a hollow structure showed better adsorptivity than did other normal nanomaterials without a hollow structure. Han et al. [17] found that hollow sub-microspheres of poly(o-phenylenediamine) (PoPD) showed enhanced adsorptivity and adsorption capacity toward Pb^{2+} when compared to solid PoPD sub-microspheres. The hollow sub-microspheres also showed good adsorptivity for other HMIs, including Hg^{2+}, Cd^{2+}, and Cu^{2+}. Meanwhile, Sun et al. [18] studied hierarchical porous, hollow, and raspberry-like TiO_2 spheres that were fabricated by adjusting the hydrolysis and condensation conditions used for synthesizing a novel amphiphilic polymeric TiO_2 precursor. The maximum Cr^{6+} adsorption capacity of the hollow spheres was larger than that the porous structure and the raspberry-like structure. Zhuang et al. [19] used a selective one-step synthesis to construct hollow spheres and found the adsorption capacity of hollow spheres toward Pb^{2+} to be larger than that of without hollow structures. Therefore, hollow micro/nanostructures can act as better adsorbents compared to other morphologies. Several hollow nanomaterials and their adsorptive properties are summarized in Table 1.

Overall, the adsorption capacity toward certain HMIs is affected not only by the nanomaterial properties, but also by the initial HMI concentration [23] as shown in Table 1. At a low initial HMI concentration, the equilibrium adsorption uptake of the adsorbents improved significantly with increasing initial HMI concentration, because the adsorption was a diffusion based process. At higher initial HMI concentrations, a greater fraction of HMIs was absorbed onto the adsorbents due to the large mass transfer

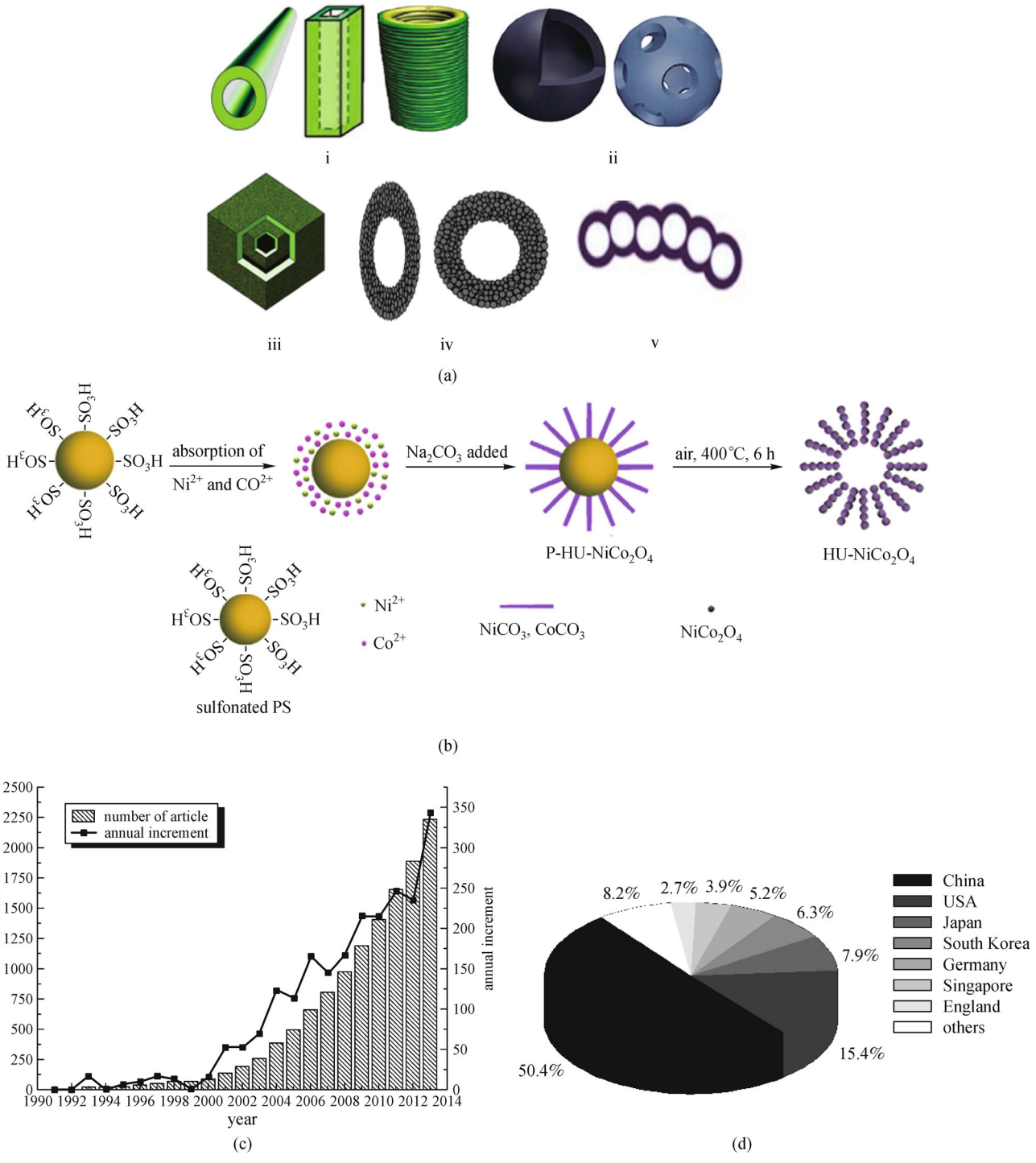

Fig. 1 (a) Hollow nanomaterials with different nanostructures (i: nanotube, ii: nanocapsule, iii: nanobox, iv: nanosphere, v: nanowire); (b) schematic illustration of the fabrication process of HU-$NiCo_2O_4$ [16];(c) time course of the publications in hollow nanomaterials research over the period 1991–2013; (d) overview of the top seven productive countries in hollow nanotechnology research over the period 1991–2013

driving force. When the HMI concentration was up to a certain value, the adsorption capacity tended to be constant because the active sites on the adsorbents were fully occupied by the HMIs [27].

In addition, organic or inorganic functionalization can improve adsorptivity and adsorption capacity [21,23,24,27]. Wang et al. [30] synthesized sym-diphenylcarbazide-functionalized silica nanotubes (SD-SNTs)

Table 1 An overview of hollow nanomaterials as applied to HMI removal

adsorbent	HMI	initial concentration /(mg·L^{-1})	surface area /(m^2·g^{-1})	adsorption capacity /(mg·g^{-1})	ref.
α-Fe_2O_3	Cr(VI)	20	11.6	7.6	[20]
$MgSiO_3$	Cr(III)	26	335.2	10.3	[19]
	Pb(II)	106	335.2	64.8	
AFCS	Cr(VI)	1000	N/A	240.0	[21]
CS	Cr(VI)	1000	N/A	175.0	
PPy nanoclusters	Cr(VI)	1000	104.0	180.4	[22]
NH_2-HCMSSs	Pb(II)	10	503.6	6.8	[23]
	Cd(II)	20		119.0	
	Zn(II)	30		194. 3	
	Pb(II)	10	503.6	6.5	
	Cd(II)	20		95.6	
	Zn(II)	30		190.3	
	Pb(II)	10	503.6	7.8	
	Cd(II)	20		98.0	
	Zn(II)	30		193.0	
thiol-SNHS	Cd(II)	2-110	823.0	15.5	[24]
	Pb(II)	1–90	823.0	17.2	
	Hg(II)	18–600	823.0	186.4	
Fe_3O_4-C	Pb(II)	1	159.8	79.0	[25]
Fe_3O_4/GO	Cr(VI)	10	N/A	27.3	[26]
SNHS	Ni(II)	100	919.0	8.4	[27]
	Cd(II)			25.9	
	Pb(II)			31.3	
NH_2-SNHS	Ni(II)	100	370.0	20.8	
	Cd(II)			31.9	
	Pb(II)			40.7	
NH_2-SG	Ni(II)	100	479.0	26.7	
	Cd(II)			54.4	
	Pb(II)			96.8	
ZnO	Ni(II)	1000	147.0	264.1	[28]
SiO_2	Pb(II)	100	291.3	260.0	[29]
	Cu(II)	100	291.3	43.6	
	Cr(III)	100	291.3	29.3	

Notes: AFCS: amino-functionalized carbon spheres, PPy nanoclusters: hierarchical porous polypyrrole nanoclusters, NH_2-HCMSSs: amino functionalized hollow core-mesoporous shell silica spheres, thiol-SNHS: thiol-functionalized silica hollow nanospheres, SNHS: unfunctionalized silica hollow nanospheres, NH_2-SNHS: amino-functionalized silica hollow nanospheres, and NH_2-SG: amino-functionalized silica gel

through the surface modification of the SNTs by sym-diphenylcarbazide and SD-SNTs showed high Pb(II) adsorption capacity as compared to SNTs, because electrostatic interactions existed in the SD-SNTs adsorption process in addition to chelating interactions. After functionalization, the well-defined tubular structure of the as-acquired SD-SNTs was retained, but the surface became smoother.

Furthermore, the recycling performance is improved by magnetization [20]. Cheng et al. [25] synthesized hollow Fe_3O_4-C nanomaterials that showed high Pb(II) adsorption capacity. Moreover, the hollow Fe_3O_4-C nanomaterials could be regenerated easily through magnetic separation at low pH.

Finally, adsorption capacity seems to be directly correlated to the covalent index between the adsorbent and HMI, and inversely correlated with charge density [29], but no explanation could be proposed.

2.2 HMI removal by photodegradation

HMIs could be removed well by adsorption, but their toxicity was not effectively degraded, and hence, secondary treatments were warranted [31]. Therefore, there is increasing interest in the photoreduction of HMIs into benign species.

Photoreduction of MMIs is based on reduction by photogenerated electrons. When a semiconductor electro-

lyte is illuminated with light energy (hv) greater than the semiconductor band gap (E_{bg}), electron/hole (h^+/e^-) pairs can be generated to photoreduce MMIs to benign species [32]. To date, photocatalysts such as ZnO, WO_3, CdS, ZnS, SnO_2, Fe_2O_3 TiO_2 and Ag have been used [33]. Based on thermodynamic analysis, only HMIs whose half-reaction standard reduction potentials are more positive than a certain value can be photoreduced [34]. The mechanism of photoreduction of HMIs is not yet clear, but the redox process can be outlined as expressed in Eqs. (2–4)

$$D \xrightarrow{hv>E_{bg}} D(h^+ + e^-) \tag{2}$$

$$M^{n+} + e^- \rightarrow M^{(n-1)+} \tag{3}$$

$$2H_2O + 4h^+ \rightarrow O_2 + 4H^+ \tag{4}$$

where D is the photocatalyst, M is the HMI, hv is light energy, and E_{bg} is the photocatalyst band gap.

Nanomaterials with a hollow structure could be promising photocatalysts for the reduction of HMIs in wastewater, because of their excellent photocatalytic activity. Li et al. [35] synthetized AgCl: Ag-hollow nanocrystals (NCs), which facilitated much faster photoreduction of Cr (VI) into the benign form that did the normal AgCl material. The special structure significantly improved light absorption and the specific surface area. Furthermore, the AgCl: Ag-hollow NCs showed excellent performance for the photoreduction of Cr(VI) into Cr(III) under visible light, which contributed to their widespread practical application.

Yang et al. [36] used TiO_2 hollow spheres to photocatalytically degrade Cr(VI) into Cr(III), which further formed oxides or hydroxides in solution. The results indicated that owing to their high specific surface area and abundant mesoporous properties, the hollow spheres show enhanced performance for the photoreduction of Cr(VI) as compared to other TiO_2 without hollow structures. Photoreduction of MMIs is a relatively new technique; because of their excellent photocatalytic properties, hollow nanomaterials are expected to play an important role in photoreducing HMIs.

3 Applications in the removal of organic pollutants

Organic pollutants, such as organic dyes and POPs, are released into water sources through industrial waste discharge, and they pose a serious threat to human health and the global environment. Nanomaterials, especially hollow nanomaterials, can remove organic pollutants owing to their excellent adsorption or photocatalytic activity. For example, Tripathi et al. [37] synthesized hollow carbon porous nanospheres (HCPNS), and then used them to synthesize silica-carbon nanospheres (Si-C) by nitrogen carbonization. HCPNSs showed a higher absorption capacity toward bisphenol A (BPA) than Si-C. Ye et al. [38] demonstrated the superior photocatalytic activity of ZnO nanocrystals with hollow structure in the degradation of tetracycline (TC) compared to nanocrystals without hollow structures (hexagonal ZnO) [38]. This is because the hollow structure and high specific surface area of the ZnO nanocrystals increases the light harvesting efficiency and the number of reaction sites [39].

3.1 Organic pollutants removal by adsorption

Hollow nanomaterials, especially hollow carbon nanomaterials such as C_{60} and carbon nanotubes (CNTs), can act as superior adsorbents for the removal of many kinds of organic pollutants, owing to their many desirable properties. In 1985, Kroto et al. [40] first reported that C_{60} could form spontaneously in carbon plasma with soccer ball structure. CNTs were first fabricated by Iijima [41] in 1991, and later extend to single-walled carbon nanotubes (SWNTs) and multi-walled carbon nanotubes (MWNTs) [42]. C_{60} and CNTs can be used to remove many kinds of organic pollutants, such as benzene, toluene, ethylbenzene [43], trihalomethanes [44], p-xylene, o-xylene [45], monoaromatic compounds and pharmaceutical antibiotics [46], mainly based on physical adsorption. To date, various models have been applied to describe the adsorption of organic contaminants on C_{60} and CNTs, such as Freundlich [47], Langmuir [48], Dubinin-Ashtakhov [49] and Polanyi-Manes [50]. Some recent papers have shown that differences exist between the maximum sorption capacities of C_{60} and CNTs for the same organic substances. For example, CNTs showed higher adsorbed volume capacity for polycyclic aromatic hydrocarbons (naphthalene, phenanthrene and pyrene) than C_{60}; furthermore, the adsorbed volume capacity of SWNTs was higher than that of MWNTs [51]. In addition, to improve the maximum sorption capacities of organic contaminates, a proper understanding of adsorption mechanisms is a key step. Different mechanisms have been proposed to explain the adsorption process, such as hydrophobic interactions, π-π bonds, electrostatic interactions and hydrogen bonds [52–54]. The dominant adsorption mechanism was not the same for different organic substances, which was of major importance for predicting organic chemical adsorption on C_{60} or CNTs. Adsorption mechanisms could be studied well by investigating the effects of the properties of both C_{60}/CNTs and organic substances in different environmental conditions [55].

Intrinsic properties of CNTs can affect the adsorption of organic contaminants. For example, Gotovac et al. [56] found the adsorption of tetracene was more than six times greater than that of phenanthrene because of the nanoscale curvature of SWCNTs. In addition, the more planar the structure of the adsorbent and the lower molecular weight of the organic contaminants, the greater would be the

adsorption capacity of C_{60} and CNTs. For example, the adsorption of $CHCl_3$ on SWCNTs is the largest among trihalomethanes owing to its lowest molecular weight [44]. Meanwhile, factors such as polarity, size, number, and location of functional groups also affected the adsorption of organic substances on C_{60} and CNTs [48,49,57].

3.2 Organic pollutants removal by photo-catalysis

Titanium dioxide (TiO_2) has attracted tremendous attention from researchers across the globe because of its low-cost, high photosensitivity and availability, nontoxicity and environment-friendliness [58]. Recent research shows that TiO_2 nanomaterials with hollow structure show higher photocatalytic activity than those without hollow structure. Zhan et al. [59] found that TiO_2 hollow fibers showed higher photocatalytic activities in the decomposition of MB than commercial TiO_2 nanoparticles without hollow structure . In this review article, we primarily focused on the application of TiO_2 hollow nanomaterials in the removal of organic pollutants.

Hollow TiO_2 nanomaterials exhibit enhanced photocatalytic properties owing to high active surface area, reduced diffusion resistance, and improved accessibility, which ensures that TiO_2 nanomaterials have enough active reaction sites for the easy approach of reactant molecules [60]. In addition, the hollow TiO_2 nanomaterials also possessed a high degree of crystallinity due to their hollow nanostructures, which was believed to improve the excitation of photo-induced electrons and the electron lifetime [61]. In addition, exposure of the TiO_2 nanomaterials to UV light results in the continuous generation of hydroxyl radicals (·OH) with strong oxidizing activity for degrading pollutants [62]. Schwarz et al. [63] found that the rate of formation of ·OH was a linear function of light intensity at low intensities. Moreover, a linear correlation also existed between the photon flux and quantum yields for the production of ·OH [64] and molecular oxygen was found to improve the formation rate of ·OH [65]. In addition, the dosage of catalyst [66], pollutants concentration [67], pH [68] and temperature [69] were found to influence the photocatalytic efficiency of TiO_2.

Hollow TiO_2 nanomaterials show excellent photocatalytic decomposition of organic hazardous substances under UV light compared to nanomaterials without hollow structures. Moreover, Syoufian et al. [70] found that TiO_2 hollow spheres absorb light at a longer wavelength compared to TiO_2 dense particles. Accordingly, hollow TiO_2 nanomaterials were considered as a promising photocatalyst, especially from the view point of the effective use of visible light (e.g., solar light). Recently, to improve the photocatalytic performance of TiO_2 hollow nanomaterials further in the removal of organic pollutants, the "Doping TiO_2" method was developed, i.e., doping pure TiO_2 with cations (e.g., Ti^{3+} [71]), and anions (e.g., nitrogen [72]), or coupling pure TiO_2 with other photocatalysts (e.g., SnO_2 [73]) and photosensitizing materials (e.g., zinc tetraaminophthalocyanine [74]).

Wang et al. [71] synthesized a superior photocatalyst by relying on a cationic Ti^{3+} self-doped yolk-shell structure. The activity of this catalyst in the degradation of Rhodamine B was tested in the visible range, and a sharp decrease of 99.3% in substrate concentration was observed within 30 min. Meanwhile, Ao et al. [72] produced anionic, nitrogen-doped TiO_2 hollow spheres (NTHS) by a one-pot hydrothermal method, using urea as the nitrogen precursor, and tested its photocatalytic activity in the degradation of Reactive Brilliant Red dye X-3B. Visible light ($\geqslant$400 nm), provided by a 290 W halogen lamp, was used as the light source. The result indicated that NTHS had a higher visible absorbance (400–700 nm), and showed a higher photocatalytic activity compared to its non-doped counterpart or commercial P25. In addition, other physical and chemical properties, such as the refractive index, hardness, electrical conductivity, and elastic modulus, were altered. Daghrir et al. found [75] the oxygen vacancies that form in TiO_2 due to nitrogen doping improve absorption in the visible region by decreasing the band gap from 3.2 to 2.6 eV.

Kim et al. [73] doped TiO_2 with another photocatalyst, developing a TiO_2/SiO_2 hollow sphere catalyst using a poly(styrene-methyl acrylic acid) matrix. This catalyst gave a photodegradation rate for methylene blue that was 2.5 times greater than that of pure TiO_2 hollow spheres.

Jiang et al. [74] also took advantage of this approach and successfully synthesized a series of zinc tetraaminophthalocyanine sensitized TiO_2 hollow nanospheres. The photocatalytic activity of this species was tested against the degradation of C.I. Basic Blue 41 under visible light, and showed almost 7 times more activity than basic TiO_2 hollow nanospheres.

4 Applications in sensors

As the world economy grows and ideas about the connection between food and health evolve, public concern about the relationship between the environment and food safety continue to increase, especially in light of continued failure to detect the contamination of consumer goods. Fortunately, hollow nanomaterials have shown potential in revealing the presence of hazardous substances. Typically, these materials are most commonly employed in the detection of HMIs and volatile organic compounds (VOCs) in the environment.

4.1 VOCs

In the last few decades, nanomaterials have been applied to the detection of H_2, CO, NO_2, NH_3, CH_4, CCl_4, ethanol, methanol, gasoline, acetone, and triethylamine [76,77]. This application has recently been extended to VOCs,

which are widely used in industrial, residential, and commercial processes and are considered major environmental pollutants. The sensing materials mainly depend on chemisorption for detecting VOCs. Several negatively charged oxygen adsorbates in air, such as O_2^-, O^-, and O^{2-} cover the nanomaterial surface, leading to a decrease in the electron density on the nanomaterial surface owing to charge transfer from the nanomaterial to the adsorbate layer. When these nanomaterials are exposed to VOCs, the negatively charged oxygen adsorbates oxidize the VOCs, leading to the release of free electrons to the nanomaterials, which results in an increase in the conductance of the nanomaterials [78].

The common method for enhancing the gas response is to hinder the process of nanomaterial aggregation, a normally strong and irreversible process relying on Van der Waals attraction. If aggregation occurs, only the resistance of the primary particles near the surface of the secondary particles is affected by exposure to reducing gases, given that the small pore size, long diffusion length, and tortuous pathway of the aggregated particles is difficult to penetrate [79]. Hollow nanomaterials are likely to improve the gas response because they provide well-defined and well-aligned micro-, meso-, and nanopores for effective gas diffusion.

Wang et al. [80] demonstrated that SnO_2 hollow microspheres had a higher sensitivity to methanol than SnO_2 nanorods did. The synthesis of these nanospheres occurs under basic conditions and is summarized in Eqs. (5–7):

$$Sn^{2+} + H_2O_2 + 4OH^- \rightarrow Sn(OH)_6^{2-} \quad (5)$$

$$Sn(OH)_6^{2-} \rightarrow SnO_2 + 2H_2O + 2OH^- \quad (6)$$

$$(CH_2)_6N_4 + 6H_2O \rightarrow 6HCHO + 4NH_3 \quad (7)$$

As seen in Fig. 2 [80], at the initial stage, small SnO_2 nanoparticles are generated by the reactions shown in Eqs. (5–6), while NH_3 is generated by the reaction shown in Eq. (7). The nanoparticles congregate around the gas and stick to each other; once the gas escapes, the hollow sphere remains.

Zhao et al. [81] took this work somewhat further, synthesizing SnO_2 hollow nanospheres that exhibited excellent ethanol sensitivity. Furthermore, they showed very high gas sensitivity – the 50 ppm ethanol concentration observed at room temperature was about 5.2 times greater than that of the corresponding nanoparticles. In addition, Martinez et al. [82] reported Sb-doped SnO_2 hollow spheres that showed gas sensitivities of 0.4–1 ppm for methanol; these values were about 3–5 times higher than those reported for SnO_2 polycrystalline chemical vapor deposition films. Furthermore, Choi et al. [83] found that the shell thickness of Fe-doped SiO_2 hollow nanomaterials also influenced the response of the sensing gas. Fe-doped SiO_2 hollow nanomaterials with a thicker shell could exhibit greater sensitivity.

4.2 HMIs

Electrochemical methods based on nanomaterials, especially hollow nanostructures, are promising for the detection of trace HMIs because of their high sensitivity, low cost, inherent simplicity, and ease of miniaturization [84]. Anodic stripping voltammetric analysis [85] and the

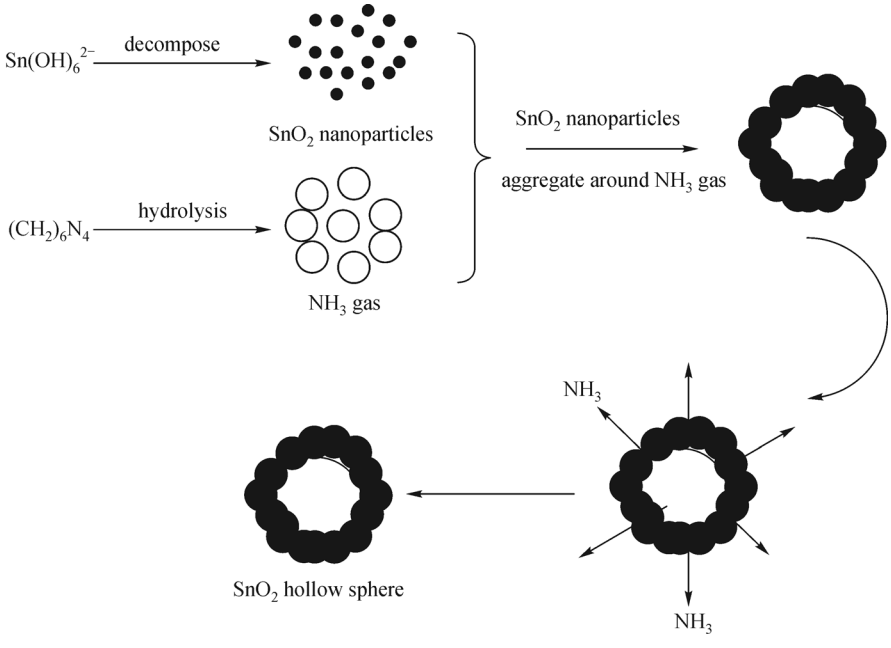

Fig. 2 Schematic of the formation of a hollow SnO_2 sphere [80]

color changes method [86] have been used as powerful tools for the detection of HMIs. Anodic stripping voltammetric analysis for the detection of HMIs mainly includes two steps: 1) reduction of HMI to HM, which accumulates onto the cathodic probe; 2) recording of the stripping voltammogram when HM is dissolved in ion form during the reverse electrode potential scan. Finally, the amount of HMI can be calculated on the basis of the voltammetric peaks. The color changes method for the detection of HMIs is based on functionalized hollow nanomaterials with a special binding group, which shows an obvious color change upon exposure to a certain HMI.

Xu et al. [85] synthesized non-conductive nanostructured magnesium silicate hollow spheres, which were useful for the individual and simultaneous electrochemical detection of HMIs, specifically Cd(II), Pb(II), Cu(II), and Hg(II) in water. Their guideline values in drinking water given by the World Health Organization (WHO) were much lower than the detection limits. Furthermore, operational parameters, such as supporting electrolytes, pH values and deposition time were also carefully studied. No obvious peak current was observed in phosphate buffer solution (PBS) and acetate buffer solution (NaAc-HAc), but a stripping peak was observed in ammonium chloride buffer solution (NH_4Cl–HCl); this difference was because the metal ions formed complexes with the supporting-electrolytes. The pH value must be considered because of its significant and predictable effect on the accumulation process of metal ions, which has a dramatic influence on the sensitivity of magnesium silicate hollow spheres. Optimum sensitivity was observed under pH 5. The accumulation step was considered a simple and effective way to enhance the sensitivity of the sensor. Therefore, the deposition time was varied from 30 to 210 s, and the peak currents increased with deposition time [85]. In addition, an interesting phenomenon of mutual interference between different metal ions was observed, i.e., the sensitivity of Pb^{2+} increasing in the presence of certain concentrations of other metal ions, such as Cd^{2+}, Cu^{2+} and Hg^{2+} is likely the most toxic of the HMIs because of its high affinity for the thiol groups in proteins and enzymes, and can damage the brain and central nervous system [87]. Cheng et al. [86] developed highly sensitive hollow sphere chemosensors, which were synthesized using sensor 2 (developed from $(Ru(\eta^6\text{-i-Pr}C_6H_6))Cl)_2$, 2-(2-thienyl)-4-hydroxymethylpyridine, KPF_6, and 3-(triethoxysilyl) propyl isocyanate) and ethyl orthosilicate in ammonia solution. The hollow sphere chemosensors could selectively indicate the presence of Hg^{2+} by forcing an immediate change in solution color from red to yellow regardless of Ni(II), Ag(I), Cr(III), Cd (II), Co(II), Pb(II), or Mn(II) concentrations of up to 1×10^{-2} moL·L^{-1}. Moreover, the adsorption capacity of the sensors remained fairly constant over a pH range of 3 to 8. These results clearly confirmed that the hollow nanomaterials have considerable potential in detecting HMIs.

5 Potential risks

Although hollow nanomaterials are promising for the purposes of environmental treatment, the risk of secondary toxicity must also be assessed.

Liu et al. [88] reported that PbO doped TiO_2 hollow spheres showed superior performance in the photocatalytic disinfection of *Escherichia coli* (*E. coli*) as compared to the unloaded samples or P25, because of the following reasons. The unique hollow structure allows for efficient light harvest by generating multiple reflections in the hollow interior voids (Fig. 3(III)) [88]. Further, the good electron trapping capability in the doped PdO results in the formation of electron trapping centers that can efficiently separate photogenerated electron/hole pairs from the photocatalyst surface to the target reactants (Fig. 3(I)) [88]. These features facilitate the production of ROS (such as ·OH radicals) to inactivate bacteria. Moreover, the PdO doping amounts for the photocatalytic disinfection of *E. coli* were studied, and the optimum PdO doping ratio (PdO/TiO_2 weight ratio) was found to be ~0.4%. At this optimum PdO doping ratio, the survival ratio of *E. coli* cells dropped significantly to ~ 1×10^{-7} after 100 min of treatment, which was far less than the ratio observed with unloaded samples or P25 (Fig. 3(II)) [88].

Liu et al. [89] found that fluorinated SnO_2 hollow nanospheres could inactivate *E. coli* K-12 efficiently through photocatalytic effects; there was no notable toxic effect of the photocatalysts used, nor did any appreciable photolysis of *E. coli* K-12 occur. Furthermore, H_2O_2 and photogenerated h^+ were considered the major reactive species responsible for inactivating *E. coli* K-12. Specifically, the inactivation kinetics could be well fitted with Eq. (8).

$$N(t) = N_0 e^{-k_{\max} t} \frac{e^{k_{\max} S}}{1 + (e^{k_{\max} S} - 1) e^{-k_{\max} t}}, \tag{8}$$

where $N_{(t)}$ and N_0 are the survival number of cells at irradiation time t and 0, respectively, $k_{\max}$ is the inactivation rate, S is the time span of initial incubation phase, and t is the irradiation time.

Fan et al. [90] found that porous Bi_2O_3 hollow nanospheres exhibited outstanding photocatalytic bactericidal performance toward *E. coli* under visible light. The reactive photo-generated oxidative species (ROS, such as-OH, $-O^{2-}$ and h^+) could attack the cell wall and membrane of *E. coli*, thus causing leakage of the intracellular content, and eventual bacterial death.

In addition, some hollow nanomaterials could even damage human cells (such as embryonic kidney (HEK293) cells [91] and human macrophage cells [92]) by oxidative stress and cytotoxicity.

Above all, hollow nano-objects can be potentially more life threatening than other common nanostructures. There-

fore, the toxicity thresholds for these materials are an important topic, and call for additional research.

6 Mechanism of hollow nanostructure formation

The synthesis methods are a bottleneck for the hollow nanomaterials. In the last few years, many attempts have been made to develop a simple, effective, controllable, and environmentally friendly method for synthesizing hollow nanomaterials. Several such techniques currently exist, including hard template, soft template, self-sacrificing template, and template-free approaches [93]. In the hard, soft, and self-sacrificing template approaches, collectively referred to as template-synthesis approaches, a sacrificial template, such as an organic/inorganic material or surfactant [16,94], is required. The hard template approach is the most common, and it involves growing the target material off the surface of a physical template, which leads to a core-shell structure; removal of the template yields the target material. Unfortunately, template removal is rather tedious and can affect the hollow structure. In contrast, the soft and self-sacrificing approaches allow for easy template removal through hydrolysis or erosion, while the template-free approach proceeds through self-assembly and eliminates the need for a template entirely. Recently, Orsi et al. [95] made the first successful attempt to produce ad hoc polymeric hollow nano-particles using a self-sacrificing template; this method is known as gas foaming. Gas foaming technology with a removable barrier film embedding the particles prior to foaming could overcome the difficulties in formatting bubble in such small-sized particles. The barrier film barrier film could stop the diffusive gas flux outside of the particle, J_{out} to retard gas loss from the free surface, so that the diffusive gas fluxes remain inside the bubble, J_{in}, and a sufficient amount of gas can accumulate for bubble formation (Fig. 4(I)) [95]. Furthermore, the removable barrier film could also contribute to the viscoelastic properties (such as the viscoelastic stresses formed by the particle, p and the interfacial tension between the materials and the air, γ thus affording a deformable confinement to the expanding polymeric particle (Fig. 4 (II)) [95]. The desired number, position, size, shape, and open/closed feature of the hollow nanostructure in the nano-particles could be produced with the proposed method.

The mechanism of hollow nanomaterial formation is particularly important, as it is a specific morphology that lends these materials their favorable properties for environmental treatment. So far, well-known mechanisms such as Ostwald ripening [96] and Kirkendall effect [97] have been applied for synthetizing hollow nano-objects. However, hollow nanomaterials fabricated by Ostwald ripening are often several hundred nanometers in size, which are unavailable the typical size for nanocrystals. Nowadays, many hollow nanomaterials are being formatted by the Kirkendall effect and the as-prepared nanocrystals are uniform in size.

The Kirkendall effect is a classical phenomenon in metallurgy. Prior to 1940s, it was normally referred to an equilibrium mutual diffusion process through the interface of coupled materials. In 1942, Kirkendall observed net mass transport across the interface of copper and brass when the temperature was elevated [98]. Copper and brass when brought in contact with each other have different diffusion rates at their interface, which leads to the net transfer of atoms across the interface.

However, the Kirkendall effect can not adequately account for the formation of hollow Pt-shell nanoparticles

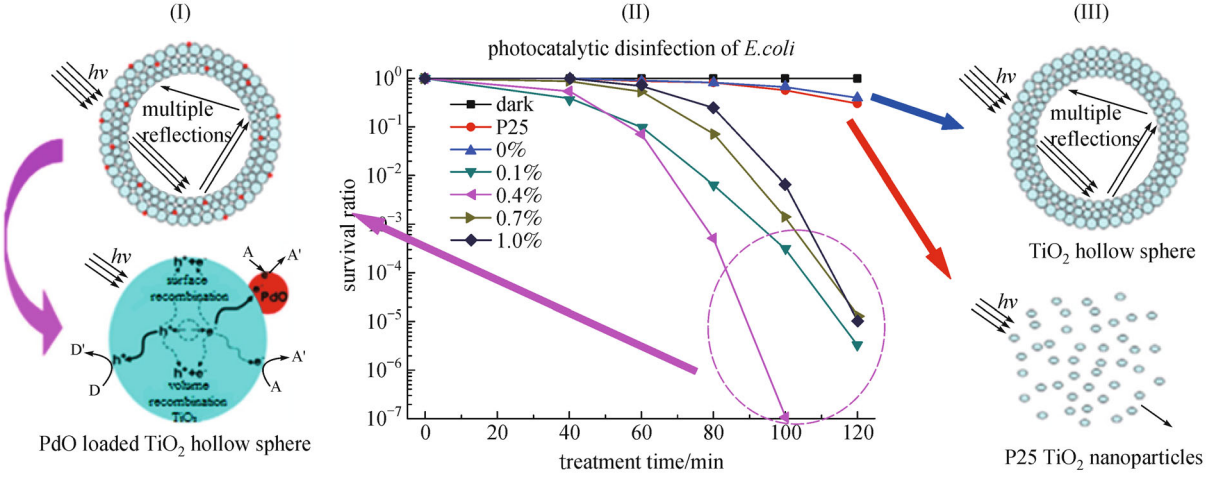

Fig. 3 The photocatalytic disinfection of *E. coli* under UV irradiation, (I) schematic illustrations for the electron/hole pair separation in the PdO doped TiO_2 hollow sphere, (II) PdO doped TiO_2 hollow sphere with different loading amounts, (III) schematic illustrations for the multiple reflections in the hollow sphere [88]

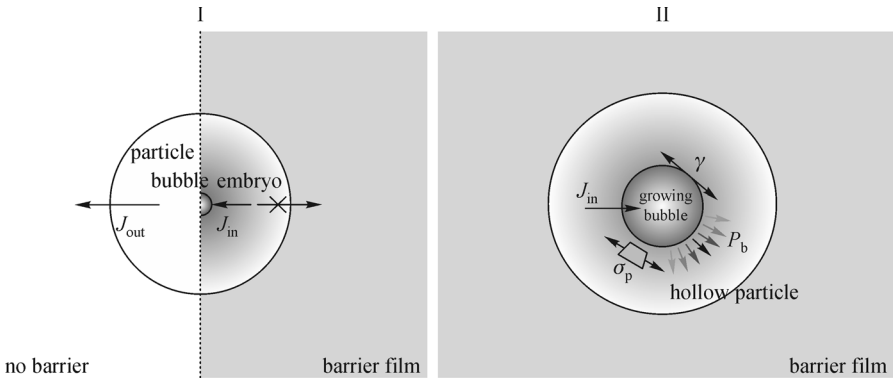

Fig. 4 Nucleation and growth mechanisms using a barrier film for the fabrication of hollow nanomaterials: (I) the barrier film makes unavailable gas diffusive path in a spherical particle, (II) the stresses acting on the growing bubble in a particle with the barrier film [95]

at room temperature [99]. It stands to reason that the mechanism for nanostructure synthesis via the Kirkendall effect would differ between room temperature and high temperature reactions. To account for this difference, Erlebacher and Margetis proposed the shape fluctuation theory, in which they introduced a quantitative model of shape fluctuation directly addressing nanoparticle stability. The model demonstrated that there is typically enough thermal energy at room temperature to excite random shape fluctuations in core-shell nanoparticles by accounting for Gibbs distribution in initial shapes.

The stages of nanostructure formation according to this model for Pt-shell nanoparticles are shown in Fig. 5 [100]. The core becomes exposed when the amplitude of thermally induced, surface diffusion-mediated random fluctuations becomes sufficiently high. At this point, pinholes form and the core dissolves; the mismatch between interior and exterior curvature in turn works as a new driving force for surface diffusion through the pinholes, resulting in their rapid closure. The closure time t_c can be determined by Eq. (9).

$$t_c = \left(\frac{\pi a R_0 k_B T}{D C_{surf} \gamma \Omega^{\frac{5}{3}}}\right)\left(a \ln\left|\frac{a}{a - r_0} - r_0\right|\right), \tag{9}$$

where a is the radius of curvature of the pinhole edge, R_0 is the radius of the sphere, k_B is the mean curvature, γ is the uniform surface energy, T is the temperature, C_{surf} is the

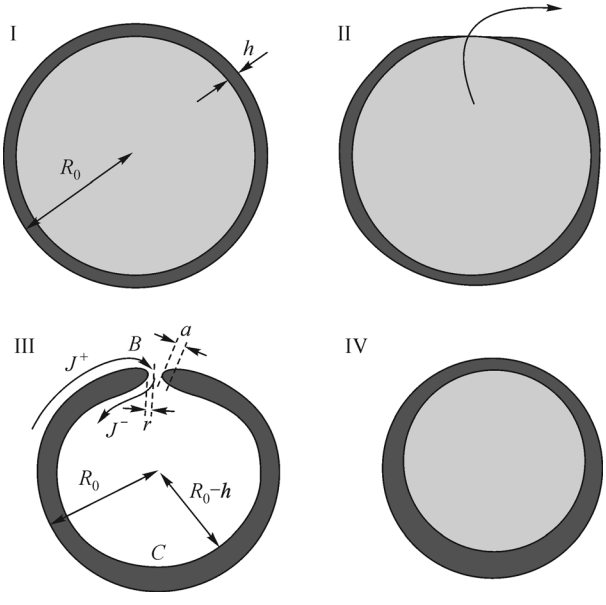

Fig. 5 The stages of nanostructure formation. (I) a core-shell nanoparticle with radius R_0 and shell thickness h; (II) the core is exposed due to shape fluctuations in the outer surface and dissolves; (III) a pinhole with radius r remains and is quickly sealed due to diffusional flux from the convex outer surface A through the pinhole edge B and into the inner concave surface C; (IV) the net flux at the pinhole edge J^+-J^- is positive, leading to an increase in the radius of the curvature of the pinhole edge a this effect accounts for the closure of the pinhole and the formation of the desired nanostructure [100]

diffusion surface concentration, D is the surface diffusion coefficient, Ω is the atomic volume, and r_0 is the radius of the pinhole.

7 Conclusions and outlook

This paper reviews different analytical techniques for nanoscale analysis and various synthetic methods for the development of hollow nanomaterials. In addition, it highlights the mechanism of hollow nanostructure formation and the application of hollow nanomaterials to the detection and removal of HMIs and organic pollutants in the environment and in food products, and concludes with some comments on the potential risk of these materials. The high chemical and thermal stability, high specific surface area, high porosity, low density, and good biocompatibility of hollow nanomaterials make them particularly promising for environmental treatment. Specifically, these materials may be essential for groundwater and soil remediation, wastewater treatment and reuse, and air purification in the near future.

However, significant challenges for the development of these materials still remain. First, improved synthetic methods that are simple, efficient, inexpensive, controllable, and environmentally friendly are required. In addition, the photocatalytic activity of these materials in the visible region must be further improved. Furthermore, integrating new properties to the currently available materials could improve their performance; for example, making them magnetic would significantly ease the recycling process. Finally, before any wide-scale application, it is imperative that further studies determine the toxicity thresholds of these materials in humans.

Acknowledgements This work was supported by the National Special Project for Science and Technology on Water Pollution Control and Management (No. 2013ZX07314-001).

References

1. Liu C. Controllable preparation of inorganic hollow nanospheres and their applications in environmental protection. Dissertation for the Doctor Degree. Zhenjiang: Jiangsu University, 2012 (in Chinese)
2. Kaur R, Hasan A, Iqbal N, Alam S, Saini M K, Raza S K. Synthesis and surface engineering of magnetic nanoparticles for environmental cleanup and pesticide residue analysis: a review. Journal of Separation Science, 2014, 37(14): 1805–1825
3. Zhang W X. Nanoscale iron particles for environmental remediation: an overview. Journal of Nanoparticle Research, 2003, 5(3–4): 323–332
4. Buzea C, Pacheco I I, Robbie K. Nanomaterials and nanoparticles: sources and toxicity. Biointerphases, 2007, 2(4): MR17–MR71
5. Aldinger F. Controlled porosity by an extreme Kirkendall effect. Acta Metallurgica, 1974, 22(7): 923–928
6. Caruso R A, Antonietti M. Sol-gel nanocoating: an approach to the preparation of structured materials. Chemistry of Materials, 2001, 13(10): 3272–3282
7. Zheng J, Wu B H, Jiang Z Y, Kuang Q, Fang X L, Xie Z X, Huang R B, Zheng L S. General and facile syntheses of metal silicate porous hollow nanostructures. Chemistry, an Asian Journal, 2010, 5(6): 1439–1444
8. Liu R M, Yin J Z, Du W D, Gao F, Fan Y Z, Lu Q Y. Monodisperse CuO Hard and Hollow Nanospheres as Visible-Light Photocatalysts. European Journal of Inorganic Chemistry, 2013, 2013(8): 1358–1362
9. Zhan S, Chen D, Jiao X, Song Y. Mesoporous TiO_2/SiO_2 composite nanofibers with selective photocatalytic properties. Chemical Communications, 2007, (20): 2043–2045
10. Yu X Y, Yu L, Shen L F, Song X H, Chen H Y, Lou X W D. General formation of MS (M = Ni, Cu, Mn) box-in-box hollow structures with enhanced pseudocapacitive properties. Advanced Functional Materials, 2014, 24(47): 7440–7446
11. Zhang F, Zhu D, Chen X, Xu X, Yang Z, Zou C, Yang K, Huang S M. A nickel hydroxide-coated 3D porous graphene hollow sphere framework as a high performance electrode material for supercapacitors. Physical Chemistry Chemical Physics, 2014, 16(9): 4186–4192
12. Wang J, Yan Y, Hojamberdiev M, Ruan X, Cai A, Xu Y. A facile synthesis of luminescent YVO_4: Eu^{3+} hollow microspheres in virtue of template function of the SDS–PEG soft clusters. Solid State Sciences, 2012, 14(8): 1018–1022
13. Shah S N, Shah S S, Ito E, Heddle J G. Template-free, hollow and porous platinum nanotubes derived from tobamovirus and their three-dimensional structure at the nanoscale. RSC Advances, 2014, 4(74): 39305–39311
14. Colder A, Huisken F, Trave E, Ledoux G, Guillois O, Reynaud C, Hofmeister H, Pippel E. Strong visible photoluminescence from hollow silica nanoparticles. Nanotechnology, 2004, 15(3): L1–L4
15. Kolmakov A. The effect of morphology and surface doping on sensitization of quasi-1D metal oxide nanowire gas sensors. Proc SPIE 2006, 6370: 63700X1–X8
16. Wang J, Qiu T, Chen X, Lu Y L, Yang W S. Hierarchical hollow urchin-like $NiCo_2O_4$ nanomaterial as electrocatalyst for oxygen evolution reaction in alkaline medium. Journal of Power Sources, 2014, 268(5): 341–348
17. Han J, Dai J, Guo R. Highly efficient adsorbents of poly (o-phenylenediamine) solid and hollow sub-microspheres towards lead ions: a comparative study. Journal of Colloid and Interface Science, 2011, 356(2): 749–756
18. Sun W, Chen M, Zhou S, Wu L. Synthesis of hierarchically nanostructured TiO_2 spheres with tunable morphologies based on a novel amphiphilic polymer precursor and their use for heavy metal ion sequestration. Journal of Materials Chemistry. A, Materials for Energy and Sustainability, 2014, 2(34): 14004–14013
19. Zhuang Y, Yang Y, Xiang G, Wang X. Magnesium silicate hollow nanostructures as highly efficient absorbents for toxic metal ions. Journal of Physical Chemistry C, 2009, 113(24): 10441–10445
20. Cheng X L, Jiang J S, Hu M, Mao G Y, Liu Z W, Zeng Y, Zhang Q H. Liquid–liquid interface-assisted solvothermal synthesis of

durian-like α-Fe_2O_3 hollow spheres constructed by nano-polyhedrons. CrystEngComm, 2012, 14(9): 3056–3062
21. Wang X, Liu J, Xu W. One-step hydrothermal preparation of amino-functionalized carbon spheres at low temperature and their enhanced adsorption performance towards Cr (VI) for water purification. Colloids and Surfaces. A, Physicochemical and Engineering Aspects, 2012, 415: 288–294
22. Yao T, Cui T, Wu J, Chen Q, Lu S, Sun K. Preparation of hierarchical porous polypyrrole nanoclusters and their application for removal of Cr (VI) ions in aqueous solution. Polymer Chemistry, 2011, 2(12): 2893–2899
23. El-Toni A M, Habila M A, Ibrahim M A, Labis J P, ALOthman Z A. Simple and facile synthesis of amino functionalized hollow core–mesoporous shell silica spheres using anionic surfactant for Pb (II), Cd (II), and Zn (II) adsorption and recovery. Chemical Engineering Journal, 2014, 251: 441–451
24. Rostamian R, Najafi M, Rafati A A. Synthesis and characterization of thiol-functionalized silica nano hollow sphere as a novel adsorbent for removal of poisonous heavy metal ions from water: kinetics, isotherms and error analysis. Chemical Engineering Journal, 2011, 171(3): 1004–1011
25. Cheng K, Zhou Y M, Sun Z Y, Hu H B, Zhong H, Kong X K, Chen Q W. Synthesis of carbon-coated, porous and water-dispersive Fe_3O_4 nanocapsules and their excellent performance for heavy metal removal applications. Dalton Transactions (Cambridge, England), 2012, 41(19): 5854–5861
26. Liu M, Wen T, Wu X, Chen C, Hu J, Li J, Wang X. Synthesis of porous Fe_3O_4 hollow microspheres/graphene oxide composite for Cr(VI) removal. Dalton Transactions (Cambridge, England), 2013, 42(41): 14710–14717
27. Najafi M, Yousefi Y, Rafati A A. Synthesis, characterization and adsorption studies of several heavy metal ions on amino-functionalized silica nano hollow sphere and silica gel. Separation and Purification Technology, 2012, 85: 193–205
28. Wang X, Cai W, Liu S, Wang G, Wu Z, Zhao H. ZnO hollow microspheres with exposed porous nanosheets surface: structurally enhanced adsorption towards heavy metal ions. Colloids and Surfaces. A, Physicochemical and Engineering Aspects, 2013, 422: 199–205
29. Liu C, Yin H B, Shi L P, Wang A L, Wu Z A, Wu G, Jiang T, Shen Y T, Jiang Y S. Adsorbability characteristic of hollow SiO_2 nanospheres for heavy metal ions. Zhongguo Youse Jinshu Xuebao, 2013, 23(6): 1661–1665 (in Chinese)
30. Wang P, Du M, Zhu H, Bao S, Yang T, Zou M. Structure regulation of silica nanotubes and their adsorption behaviors for heavy metal ions: pH effect, kinetics, isotherms and mechanism. Journal of Hazardous Materials, 2015, 286: 533–544
31. Liu G, Deng Q, Wang H M, Kang S H, Yang Y, Ng D H L, Cai W P, Wang G. Z. Synthesis and characterization of nanostructured Fe_3O_4 micron-spheres and their application in removing toxic Cr ions from polluted water 2012, 18(42): 13418–13426
32. Colón G, Hidalgo M C, Navío J A. Photocatalytic deactivation of commercial TiO_2 samples during simultaneous photoreduction of Cr(VI) and photooxidation of salicylic acid. Journal of Photochemistry and Photobiology A Chemistry, 2001, 138(1): 79–85
33. Bhatkhande D S, Pangarkar V G, Beenackers A A C M. Photacatalytic degradation for environmental applicatons-a review. Journal of Chemical Technology and Biotechnology (Oxford, Oxfordshire), 2002, 77(1): 102–116
34. Huang J Y, Liu G H, Zhang W H, Huang J, Lin T, Wang Y J. Progress on photocatalytic reduction of heavy metal ions in wastewater. Environmental Science & Technology, 2008, 31(12): 104–108(in Chinese)
35. Li H Y, Wu T S, Cai B, Ma W G, Sun Y J, Gan S Y, Han D X, Niu L. Efficiently photocatalytic reduction of carcinogenic contaminant Cr(VI) upon robust AgCl:Ag hollow nanocrystals. Applied Catalysis B: Environmental, 2015, 164: 344–351
36. Yang Y, Wang G, Deng Q, Wang H, Zhang Y, Ng D H, Zhao H. Enhanced photocatalytic activity of hierarchical structure TiO_2 hollow spheres with reactive (001) facets for the removal of toxic heavy metal Cr(VI). RSC Advances, 2014, 4(65): 34577–34583
37. Tripathi P K, Gan L, Liu M, Ma X M, Zhao Y H, Zhu D Z, Xu Z J, Chen L W, Rao N N. One-pot assembly of silica@ two polymeric shells for synthesis of hollow carbon porous nanospheres: adsorption of bisphenol A. Materials Letters, 2014, 120: 108–110
38. Ye L, Guan W, Lu C, Zhao H, Lu X. Fabrication of hollow ZnO hexahedral nanocrystals grown on Si (100) substrate by a facile route. Materials Letters, 2014, 118: 115–118
39. Liu J, Zhang G K, Yu J C, Guo Y D. In situ synthesis of Zn_2GeO_4 hollow spheres and their enhanced photocatalytic activity for the degradation of antibiotic metronidazole. Dalton Transactions (Cambridge, England), 2013, 42(14): 5092–5099
40. Kroto H W, Heath J R, O'Brien S C, Curl R F, Smalley R E. C_{60}: Buckminsterfullerene.. Nature, 1985, 318(6042): 162–163
41. Iijima S. Helical microtubules of graphitic carbon. Nature, 1991, 354(6348): 56–58
42. Ong Y T, Ahmad A L, Zein S H S, Tan S H. A review on carbon nanotubes in an environmental protection and green engineering perspective. Brazilian Journal of Chemical Engineering, 2010, 27 (2): 227–242
43. Su F, Lu C, Hu S. Adsorption of benzene, toluene, ethylbenzene and p-xylene by NaOCl-oxidized carbon nanotubes. Colloids and Surfaces. A, Physicochemical and Engineering Aspects, 2010, 353 (1): 83–91
44. Lu C, Chung Y L, Chang K F. Adsorption of trihalomethanes from water with carbon nanotubes. Water Research, 2005, 39(6): 1183–1189
45. Chin C J M, Shih L C, Tsai H J, Liu T K. Adsorption of o-xylene and p-xylene from water by SWCNTs. Carbon, 2007, 45(6): 1254–1260
46. Ji L L, Shao Y, Xu Z Y, Zheng S R, Zhu D Q. Adsorption of monoaromatic compounds and pharmaceutical antibiotics on carbon nanotubes activated by KOH etching. Environmental Science & Technology, 2010, 44(16): 6429–6436
47. Lin D H, Xing B S. Adsorption of phenolic compounds by carbon nanotubes: role of aromaticity and substitution of hydroxyl groups. Environmental Science & Technology, 2008, 42(19): 7254–7259
48. Liao Q, Sun J, Gao L. The adsorption of resorcinol from water using multi-walled carbon nanotubes. Colloids and Surfaces. A, Physicochemical and Engineering Aspects, 2008, 312(2–3): 160–165
49. Yang K, Wu W, Jing Q, Zhu L. Aqueous adsorption of aniline,

phenol, and their substitutes by multi-walled carbon nanotubes. Environmental Science & Technology, 2008, 42(21): 7931–7936
50. Pan B, Lin D H, Mashayekhi H, Xing B S. Adsorption and hysteresis of bisphenol A and 17 alpha-ethinyl estradiol on carbon nanomaterials. Environmental Science & Technology, 2008, 42 (15): 5480–5485
51. Yang K, Zhu L, Xing B. Adsorption of polycyclic aromatic hydrocarbons by carbon nanomaterials. Environmental Science & Technology, 2006, 40(6): 1855–1861
52. Coughlin R W, Ezra F S. Role of surface acidity in the adsorption of organic pollutants on the surface of carbon. Environmental Science & Technology, 1968, 2(4): 291–297
53. Mattson J A, Mark H B Jr, Malbin M D, Weber W J Jr, Crittenden J C. Surface chemistry of active carbon: specific adsorption of phenols. Journal of Colloid and Interface Science, 1969, 31(1): 116–130
54. Chen W, Duan L, Wang L, Zhu D. Adsorption of hydroxyl-and amino-substituted aromatics to carbon nanotubes. Environmental Science & Technology, 2008, 42(18): 6862–6868
55. Pan B, Xing B. Adsorption mechanisms of organic chemicals on carbon nanotubes. Environmental Science & Technology, 2008, 42 (24): 9005–9013
56. Gotovac S, Honda H, Hattori Y, Takahashi K, Kanoh H, Kaneko K. Effect of nanoscale curvature of single-walled carbon nanotubes on adsorption of polycyclic aromatic hydrocarbons. Nano Letters, 2007, 7(3): 583–587
57. Lin D, Xing B. Adsorption of phenolic compounds by carbon nanotubes: role of aromaticity and substitution of hydroxyl groups. Environmental Science & Technology, 2008, 42(19): 7254–7259
58. Ghasemzadeh G, Momenpour M, Omidi F, Hosseini M R, Ahani M, Barzegari A. Applications of nanomaterials in water treatment and environmental remediation. Frontiers of Environmental Science and Engineering, 2014, 8(4): 1–12
59. Zhan S H, Chen D R, Jiao X L, Tao C H. Long TiO_2 hollow fibers with mesoporous walls: sol-gel combined electrospun fabrication and photocatalytic properties. Journal of Physical Chemistry B, 2006, 110(23): 11199–11204
60. Joo J B, Dahl M, Li N, Zaera F, Yin Y. Tailored synthesis of mesoporous TiO_2 hollow nanostructures for catalytic applications. Energy & Environmental Science, 2013, 6(7): 2082–2092
61. Bard A J. Photoelectrochemistry and heterogeneous photocatalysis at semiconductors. Journal of Photochemistry, 1979, 10 (1): 59–75
62. Amalric L, Guillard C, Pichat P. Use of catalase and superoxide dismutase to assess the roles of hydrogen peroxide and superoxide in the TiO_2 or ZnO photocatalytic destruction of 1, 2-dimethoxybenzene in water. Research on Chemical Intermediates, 1994, 20 (6): 579–594
63. Schwarz P F, Turro N J, Bossmann S H, Braun A M, Wahab A M A A, Dürr H. A new method to determine the generation of hydroxyl radicals in illuminated TiO_2 suspensions. Journal of Physical Chemistry B, 1997, 101(36): 7127–7134
64. Grela M A, Coronel M E J, Colussi A J. Quantitative spin-trapping studies of weakly illuminated titanium dioxide sols. Implications for the mechanism of photocatalysis. Journal of Physical Chemistry, 1996, 100(42): 16940–16946
65. Fukahori S, Ichiura H, Kitaoka T, Tanaka H. Photocatalytic decomposition of bisphenol A in water using composite TiO_2-zeolite sheets prepared by a papermaking technique. Environmental Science & Technology, 2003, 37(5): 1048–1051
66. Li X X, Fang S M, Ge L, Han C C, Qiu P, Liu W L. Synthesis of flower-like Ag/AgCl-Bi_2MoO_6 plasmonic photocatalysts with enhanced visible-light photocatalytic performance. Applied Catalysis B: Environmental, 2015, 176–177: 162–169
67. Kanki T, Yoneda H, Sano N, Toyoda A, Nagai C. Photocatalytic reduction and deposition of metallic ions in aqueous phase. Chemical Engineering Journal, 2004, 97(1): 77–81
68. Kyung H, Lee J, Choi W. Simultaneous and synergistic conversion of dyes and heavy metal ions in aqueous TiO_2 suspensions under visible-light illumination. Environmental Science & Technology, 2005, 39(7): 2376–2382
69. Hsiao C Y, Lee C L, Ollis D F. Heterogeneous photocatalysis: degradation of diluted solutions of dichloromethane (CH_2Cl_2), chloroform ($CHCl_3$) and carbon tetrachloride (CCl_4) with illuminated TiO_2 photocatalyst. Journal of Catalysis, 1983, 82(2): 418–423
70. Syoufian A, Satriya O H, Nakashima K. Photocatalytic activity of titania hollow spheres: photodecomposition of methylene blue as a target molecule. Catalysis Communications, 2007, 8(5): 755–759
71. Wang S X, Yang X J, Wang Y P, Liu L X, Guo Y Y, Guo H. Morphology-controlled synthesis of Ti^{3+} self-doped yolk–shell structure titanium oxide with superior photocatalytic activity under visible light. Journal of Solid State Chemistry, 2014, 213(5): 98–103
72. Ao Y, Xu J, Zhang S, Fu D. A one-pot method to prepare N-doped titania hollow spheres with high photocatalytic activity under visible light. Applied Surface Science, 2010, 256(9): 2754–2758
73. Kim H R, Choi K Y, Shul Y G. Preparation of TiO_2/SiO_2 hollow spheres and their activity in methylene blue photodecomposition. Korean Journal of Chemical Engineering, 2007, 24(4): 596–599
74. Jiang Y, Guo L, Zhang W, Dai F, Yan Y, Zhang F, Lv H. Preparation of zinc tetraaminophthalocyanine sensitized TiO_2 hollow nanospheres and their enhanced photocatalytic properties under visible light. Desalination and Water Treatment, 2013 (ahead-of-print): 1–8
75. Daghrir R, Drogui P, Robert D. Modified TiO_2 for environmental photocatalytic applications: a review. Industrial & Engineering Chemistry Research, 2013, 52(10): 3581–3599
76. Zhang J, Wang S, Wang Y, Wang Y, Zhu B L, Xia H J, Guo X Z, Zhang S M, Huang W P, Wu S H. NO_2 sensing performance of SnO_2 hollow-sphere sensor. Sensors and Actuators. B, Chemical, 2009, 135(2): 610–617
77. Ju D, Xu H, Qiu Z, Guo J, Zhang J, Cao B. Highly sensitive and selective triethylamine-sensing properties of nanosheets directly grown on ceramic tube by forming NiO/ZnO PN heterojunction. Sensors and Actuators. B, Chemical, 2014, 200: 288–296
78. Liu J, Wang X, Peng Q, Li Y. Preparation and gas sensing properties of vanadium oxide nanobelts coated with semiconductor oxides. Sensors and Actuators. B, Chemical, 2006, 115(1): 481–487
79. Lee J H. Gas sensors using hierarchical and hollow oxide nanostructures: overview. Sensors and Actuators. B, Chemical,

2009, 140(1): 319–336
80. Wang H Z, Liang J B, Fan H, Xi B J, Zhang M F, Xiong S L, Zhu Y C, Qian Y T. Synthesis and gas sensitivities of SnO_2 nanorods and hollow microspheres. Journal of Solid State Chemistry, 2008, 181 (1): 122–129
81. Zhao Q R, Gao Y, Bai X, Wu C Z, Xie Y. Facile synthesis of SnO_2 hollow nanospheres and applications in gas sensors and electrocatalysts. European Journal of Inorganic Chemistry, 2006, 2006(8): 1643–1648
82. Martinez C J, Hockey B, Montgomery C B, Semancik S. Porous tin oxide nanostructured microspheres for sensor applications. Langmuir, 2005, 21(17): 7937–7944
83. Choi W S, Koo H Y, Zhongbin Z, Li Y, Kim D Y. Templated synthesis of porous capsules with a controllable surface morphology and their application as gas sensors. Advanced Functional Materials, 2007, 17(11): 1743–1749
84. Herzog G, Beni V. Stripping voltammetry at micro-interface arrays: A review. Analytica Chimica Acta, 2013, 769: 10–21
85. Xu R X, Yu X Y, Gao C, Jiang Y J, Han D D, Liu J H, Huang X J. Non-conductive nanomaterial enhanced electrochemical response in stripping voltammetry: the use of nanostructured magnesium silicate hollow spheres for heavy metal ions detection. Analytica Chimica Acta, 2013, 790: 31–38
86. Cheng X, Li J, Li X, Zhang D H, Zhang H J, Zhang A Q, Huang H, Lian J S. A highly sensitive sensor based on hollow particles for the detection, adsorption and removal of Hg^{2+} ions. Journal of Materials Chemistry, 2012, 22(45): 24102–24108
87. Harris H H, Pickering I J, George G N. The chemical form of mercury in fish. Science, 2003, 301(5637): 1203–1203
88. Liu Y, Li Q, Zhang J T, Sun W Z, Gao S A, Shang J K. PdO loaded TiO_2 hollow sphere composite photocatalyst with a high photocatalytic disinfection efficiency on bacteria. Chemical Engineering Journal, 2014, 249: 63–71
89. Liu S W, Huang G C, Yu J G, Ng T W, Yip H Y, Wong P K. Porous fluorinated SnO_2 hollow nanospheres: transformative selfassembly and photocatalytic inactivation of bacteria. ACS Applied Materials & Interfaces, 2014, 6(4): 2407–2414
90. Qin F, Zhao H P, Li G F, Yang H, Li J, Wang R M, Liu Y L, Hu J C, Sun H Z, Chen R. Size-tunable fabrication of multifunctional Bi_2O_3 porous nanospheres for photocatalysis, bacteria inactivation and template-synthesis. Nanoscale, 2014, 6(10): 5402–5409
91. Reddy A R N, Reddy Y N, Krishna D R, Himabindu V. Multi wall carbon nanotubes induce oxidative stress and cytotoxicity in human embryonic kidney (HEK293) cells. Toxicology, 2010, 272 (1–3): 11–16
92. Cheng C, Müllerb K H, Koziol K K K, Skepperb J N, Midgley P A, Welland M E, Porter A E. Toxicity and imaging of multi-walled carbon nanotubes in human macrophage cells. Biomaterials, 2009, 30(25): 4152–4160
93. Kang X, Li C, Cheng Z, Ma P A, Hou Z, Lin J. Lanthanide-doped hollow nanomaterials as theranostic agents. Wiley Interdisciplinary Reviews. Nanomedicine and Nanobiotechnology, 2014, 6(1): 80–101
94. Pei J, Chen G, Jia D, Yu Y, Sun J, Qiu Z, Yu Y. Construction of hollow tellurium hierarchical architecture via a trisodium citrate assisted self-sacrificed template eroding mechanism. RSC Advances, 2014, 4(68): 36257–36261
95. Orsi S, Di Maio E, Iannace S, Netti P A. Hollow micro-and nanoparticles by gas foaming. Nano Research, 2014, 7(7): 1018–1026
96. Wu L, Qiao X, Cui S, Hong Z, Fan X. Synthesis of monolithic aerogel-like alumina via the accumulation of mesoporous hollow microspheres. Microporous and Mesoporous Materials, 2015, 202: 234–240
97. Guo J, Zhang X, Zhang T, Zhou T, Zhang X, Quan Z. Self-template synthesis of magnetic cobalt nanotube based on Kirkendall effect. Materials Letters, 2015, 141: 288–290
98. Huang T, Qi L M. Solution-phase synthesis of inorganic nanostructures by chemical transformation from reactive templates. Science China Chemistry, 2010, 53(2): 365–371
99. Lopez-Haro M, Dubau L, Guétaz L, Bayle-Guillemaud P, Chatenet M, Andre J, Caque N, Rossinot E, Maillard F. Atomic-scale structure and composition of Pt_3Co/C nanocrystallites during real PEMFC operation: a STEM–EELS study. Applied Catalysis B: Environmental, 2014, 152–153: 300–308
100. Erlebacher J, Margetis D. Mechanism of hollow nanoparticle formation due to shape fluctuations. Physical Review Letters, 2014, 112(15): 155505